Scaling Law for the Onset of Solidification at Extreme Undercooling

Philip C. Myint[1,*] Dane M. Sterbentz[1,2,*] Justin L. Brown,[3] Brian S. Stoltzfus,[3]
Jean-Pierre R. Delplanque,[2] and Jonathan L. Belof[1,†]

[1]*Lawrence Livermore National Laboratory, Livermore, California 94550, USA*
[2]*Department of Mechanical & Aerospace Engineering, University of California, Davis, California 95616, USA*
[3]*Sandia National Laboratories, Albuquerque, New Mexico 87185, USA*

Quasi-isentropic compression enables one to study the solidification of metastable liquid states that are inaccessible through other experimental means. The onset of this nonequilibrium solidification is known to depend on the compression rate and material-specific factors, but this complex interdependence has not been well characterized. In this study, we use a combination of experiments, theory, and computational simulations to derive a general scaling law that quantifies this dependence. One of its applications is a novel means to elucidate melt temperatures at high pressures.

Quasi-isentropic (e.g., ramp) compression has emerged as a powerful means to probe the behavior of matter at extreme conditions that lie at the frontier of knowledge in modern science [1,2]. The relatively low rates of entropy generation and extremely rapid nature of the compression process has made it an ideal technique to examine the thermodynamics and kinetics of phase transitions, especially solidification, that occur under far-from-equilibrium conditions [3–6]. For such first-order phase transitions, the reordering of matter occurs via a process of nucleation and growth [7–11]. In particular, the solidification of metallic or molecular materials is known to be greatly influenced by the degree to which the system is undercooled beyond the equilibrium melt curve. As the magnitude of undercooling is increased (typically accomplished by imposing a variation in cooling rate but can also be attained via volumetric compression) the nucleation rate can be tremendously enhanced, resulting in reduced grain size, altered morphology, and the appearance of metastable structures along the transition path. Through application of the principles governing nucleation far from equilibrium, the ability to engineer materials with specific properties—by utilizing control over the nonequilibrium path—comes into view.

Three types of experimental quasi-isentropic loading platforms have been used to investigate nonequilibrium solidification kinetics: those involving (i) laser drives [12,13]; (ii) magnetic drives [14,15]; and (iii) gas guns [16,17]. For a given target sample and initial state, the thermodynamic path

followed in all three platforms is the same [Fig. 1(a)], barring small differences due to experimental uncertainties and relatively modest variations in the amount of entropy generation (i.e., in the deviation between the quasi-isentrope and the actual isentrope). However, the compression rate dP/dt with which this path is traversed differs drastically—by 2 orders of magnitude—among the three platforms [Fig. 1(b)]. The phase transition often appears in velocimetry traces as a brief transient pullback in the pressure (due to the newly formed solid having a higher density than the original liquid phase), and the pressure P_{trans} at the peak of this pullback loop, which far exceeds the equilibrium melt pressure P_{melt} and is commonly interpreted to be at or near the onset time for the nonequilibrium solidification of metastable liquid, tends to increase with dP/dt. This implies that P_{trans} depends not only on the physical conditions along the compression path, but also on how fast those conditions are traversed; a fact that has puzzled researchers to this day.

Modern studies of solidification kinetics under quasi-isentropic compression have focused on water [4,6,18–23], and it is known from these studies that solidification to the high-pressure ice VII phase is dominated by homogeneous nucleation if P_{trans} is at least about 6 GPa. The primary aim of our work is to provide a quantitative explanation of the dependence of P_{trans} under homogeneous nucleation on dP/dt, culminating in a general scaling law that is applicable to water and to other materials as well.

Our scaling law rests on the foundation of the published data on water [4,6,18–23], plus our own magnetic-drive experiments on the solidification of gallium (Ga) to the Ga-III phase that are depicted in Fig. 1(c) and are described in more detail in the Supplemental Material [24]. Because Ga has very different properties than water (e.g., monatomic metal vs molecular insulator), a scaling law that can describe both materials may therefore be applicable to a
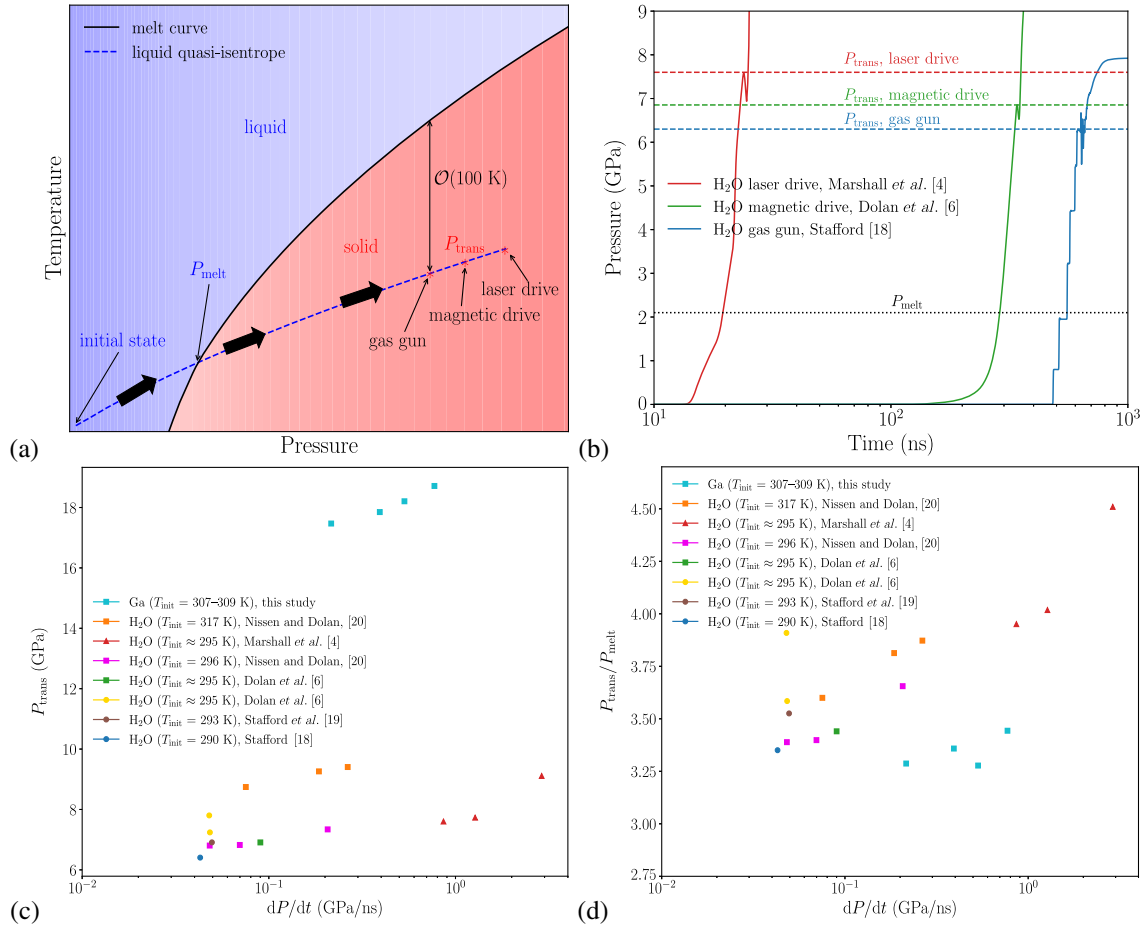
FIG. 1. Different quasi-isentropic loading platforms (laser drives, magnetic drives, gas guns) traverse roughly the same compression path, but at significantly different rates dP/dt, with faster rates tending to increase the nonequilibrium transition pressure P_{trans} where solidification becomes macroscopically observable: (a) schematic illustration of the temperature-pressure path (the thick arrows indicate the direction along this path) followed in quasi-isentropic loading, showing the sensitivity of P_{trans} to dP/dt; (b) pressure vs time in simulations of three experiments on water [4,6,18] that all start at ambient conditions, but each conducted with a different quasi-isentropic loading platform; (c) P_{trans} vs dP/dt for various studies on water [4,6,18–20] and our own magnetic-drive experiments on gallium (Ga), in all of which the transition occurs primarily through homogeneous nucleation; (d) same as in (c), except that P_{trans} is normalized by the equilibrium melt pressure P_{melt} at which the corresponding isentrope intersects the melt curve (solid-liquid equilibrium phase boundary). Note that all of the studies on water are nominally initiated from room temperature, except for the three Nissen and Dolan [20] points colored in orange, which involve preheated water samples where the initial temperature $T_{\text{init}} = 317$ K. In (c) and (d), as well as in all subsequent figures, the triangles, squares, and circles denote experiments conducted with laser drives, magnetic drives, and gas guns, respectively. Ice VII is formed in all the water experiments, while Ga-III is formed in our Ga experiments.

wide variety of materials under quasi-isentropic compression. Furthermore, the Ga data present an interesting challenge: Figure 1(d) suggests that normalizing P_{trans} with the melt pressure P_{melt} can largely account for differences in P_{trans} due to the choice of the initial temperature T_{init}, but it clearly cannot capture material-specific differences that exist between water and Ga.

We develop the scaling law for P_{trans} by applying the well-known technique of dimensional analysis [39,40]. A necessary first step in dimensional analysis (see the Supplemental Material [24] for more details) is to ascribe

a physical framework to the problem of interest, and for this purpose, we employ models based on classical nucleation theory (CNT) and growth [7–11]. According to CNT, solidification is controlled by the liquid-solid interfacial free energy σ, the density ρ of the liquid, as well as the temperature T and pressure P. A natural choice that we follow is to use the equilibrium melt values of these properties [i.e., properties evaluated at the intersection point of the isentrope with the melt curve; this point is indicated by P_{melt} in Fig. 1(a)] as characteristic values in the nondimensionalization. By simplifying the problem down
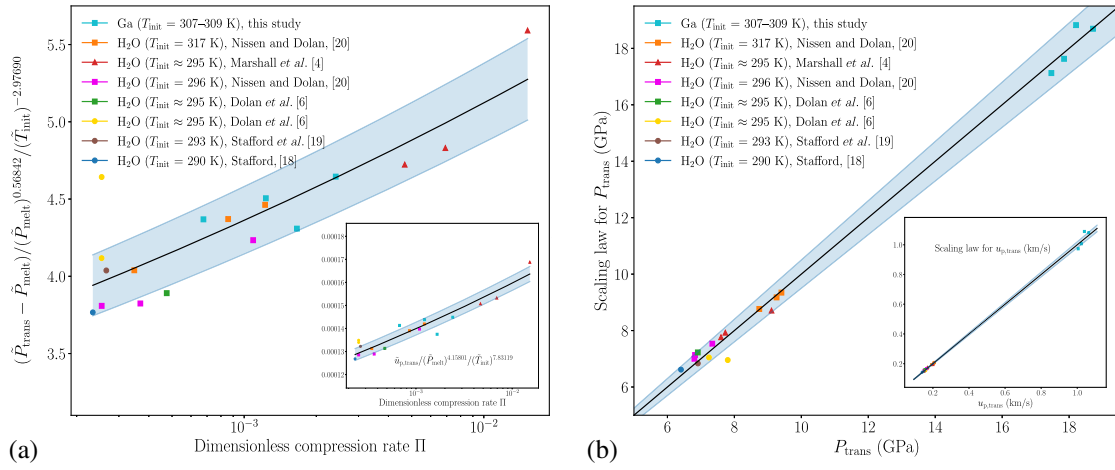
FIG. 2. Illustration of the scaling law: (a) in nondimensionalized terms, where the y-axis label is just a rearrangement of Eq. (1) and represents the "projection" of the dimensionless transition pressure $\tilde{P}_{\text{trans}}$ on the dimensionless compression rate Π; (b) P_{trans} predicted by the scaling law vs the actual value. The black line in (b), which is simply a plot of $y = x$, indicates a perfect prediction. The insets in these figures show the results of applying the same dimensional analysis to the particle speed $u_{\text{p,trans}}$, which leads to the scaling law $\tilde{u}_{\text{p,trans}} = u_{\text{p,trans}}/(RT_{\text{melt}})^{1/2} = 0.000208(\Pi)^{0.05751}(\tilde{P}_{\text{melt}})^{4.15801}(\tilde{T}_{\text{init}})^{7.83119}$. The blue bands indicate $\pm 5\%$ and $\pm 2\%$ intervals centered around the black curves for the transition pressure $\tilde{P}_{\text{trans}}$ and particle speed $\tilde{u}_{\text{p,trans}}$, respectively.

to its essence, the dimensional analysis reveals that the nondimensionalized transition pressure $\tilde{P}_{\text{trans}} = P_{\text{trans}}/(\rho_{\text{melt}}RT_{\text{melt}})$ is a function of just three dimensionless parameters: (i) the compression rate $\Pi = (dP/dt)/[\rho_{\text{melt}}^2\sigma_{\text{melt}}^{-1}(RT_{\text{melt}})^{5/2}]$, (ii) the initial temperature $\tilde{T}_{\text{init}} = T_{\text{init}}/T_{\text{melt}}$, and (iii) the melt pressure $\tilde{P}_{\text{melt}} = P_{\text{melt}}/(\rho_{\text{melt}}RT_{\text{melt}})$, where R is the gas constant expressed per unit mass. Nucleation and growth processes also depend on bulk chemical potential (free energy) differences between liquid and solid, which we denote as $\Delta\mu$, but the conundrum here is that with our choice to use equilibrium melt properties as characteristic values in the dimensional analysis, $\Delta\mu$ becomes trivial because $\Delta\mu_{\text{melt}} = 0$ by definition. However, as discussed further in the Supplemental Material [24], the relative difference between T_{init} and T_{melt} gives a sense of how large $\Delta\mu$ is at the transition pressure (smaller differences between T_{init} and T_{melt} are correlated with smaller values of $\Delta\mu$), and so we use the nondimensionalized initial temperature $\tilde{T}_{\text{init}} = T_{\text{init}}/T_{\text{melt}}$ as a nontrivial surrogate for $\Delta\mu$. The Supplemental Material [24] also describes how we apply our constitutive models (those pertaining to phase-transition kinetics, equations of state, interfacial free energy) and our kinetics code Samsa developed over the past several years [5,41–47] to simulate all of the experiments in Fig. 1, calculate relevant quantities, and execute the dimensional analysis. Doing so yields the following scaling law depicted in Fig. 2:

$$\tilde{P}_{\text{trans}} = \tilde{P}_{\text{melt}} + 7.06298(\Pi)^{0.06976}(\tilde{P}_{\text{melt}})^{0.56842}(\tilde{T}_{\text{init}})^{-2.97690}.$$

(1)

Comparing the "raw" data in Fig. 1(c) with the transformed results in Fig. 2, we see that the scaling law in Eq. (1)

quantifies the observed transition pressure P_{trans} in both water and Ga under the vastly different compression rates exhibited in laser-drive, magnetic-drive, and gas-gun experiments. Because it apparently normalizes out material-specific differences between water and Ga—two very different kinds of substances—this suggests that the scaling law, perhaps after additional refinement as more data become available, may be used to predict P_{trans} in quasi-isentropic compression experiments on a wide range of materials so long as their equilibrium melt properties (P_{melt}, σ_{melt}, ρ_{melt}, and T_{melt}) are known, and the phase transition is well described by CNT.

The fact that the same solidification process is observable across the three types of experimental platforms (laser drives, magnetic drives, gas guns) considered in our study, even though these different platforms access timescales that can differ by over 2 orders of magnitude, clearly suggests that the compression rate influences the observed kinetics of the phase transition. The precise mechanistic details as to how this compression-rate dependence arises warrant further investigation through atomistic simulations, but CNT already provides valuable insight into this. Intuitively, it stands to reason that higher compression rates allow the metastable liquid to be undercooled further along the quasi-isentrope [see Fig. 1(a)] because equilibrium restoring forces (i.e., those that are trying to cause solidification) have less time to act. Larger undercooling means that $\Delta\mu/k_BT$ at the transition time increases with dP/dt, where $\Delta\mu$ is the chemical potential difference between liquid and solid, and k_B is the Boltzmann constant. As a result, the nucleation energy barrier $\Delta G^*/k_BT = 16\pi\sigma^3/[3k_BT(\rho\Delta\mu)^2]$ must decrease with dP/dt, as shown in Fig. 3(a). CNT gives the nucleation rate as
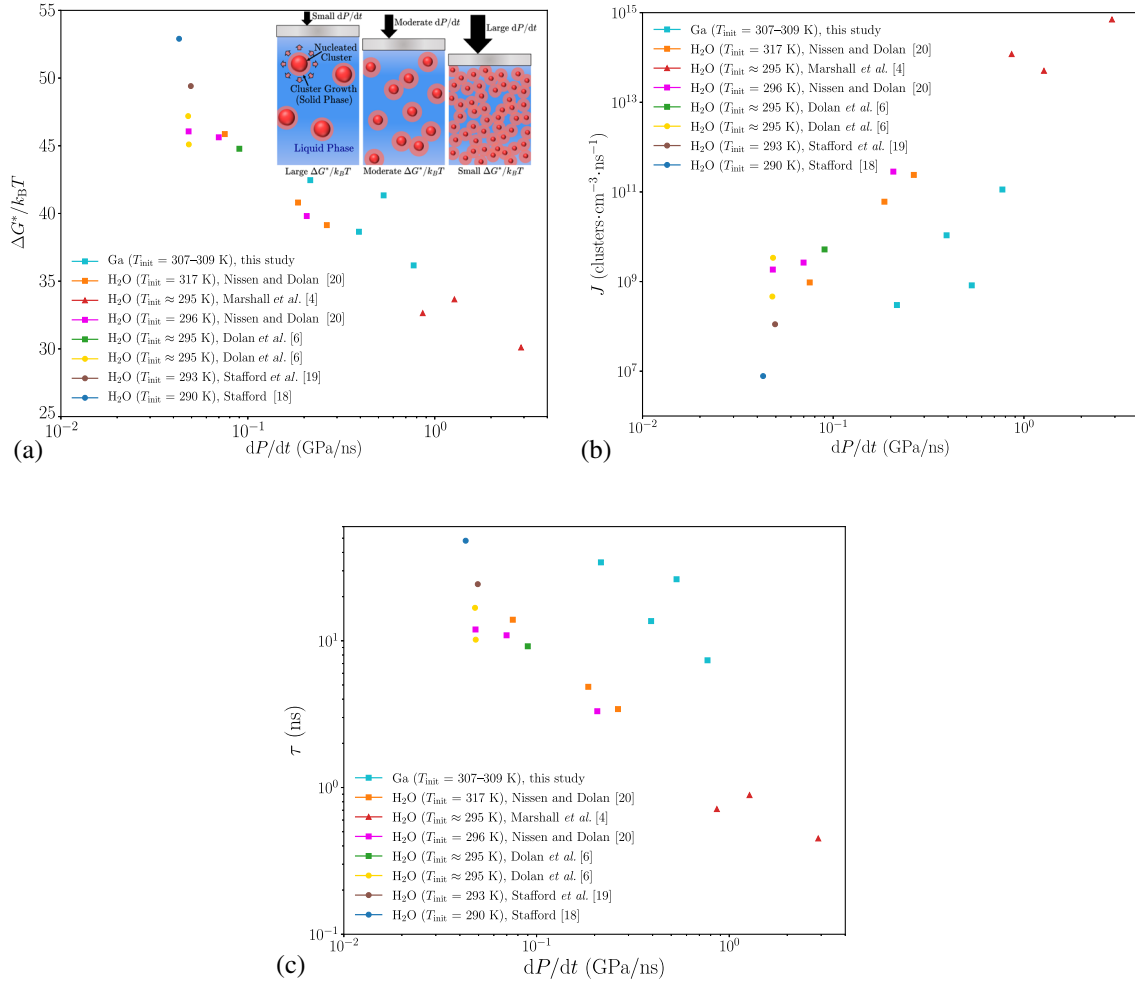
FIG. 3. Demonstration of the increased extent of undercooling with higher compression rates, where the quantities in this figure are evaluated at the time in our simulations of each experiment where the nucleation rate J attains a peak value (this maximum is almost coincident with, but occurs slightly earlier than when P_{trans} is achieved): (a) the nucleation energy barrier $\Delta G^*/k_B T$; (b) the nucleation rate J; (c) Kolmogorov time $\tau = (\pi J \gamma^3/3)^{-1/4}$. Here, γ is the growth rate of the nucleated solid clusters. If J and γ were held fixed at some constant set of values, the solid phase fraction ϕ would increase with time t according to $\phi = 1 - \exp[-(t/\tau)^4]$, and so τ represents a characteristic time of the phase transition. The growth rate is given by $\gamma = (RT)^{1/2}[1 - \exp(-\Delta\mu/k_B T)]$, and unlike J—which varies by nearly a factor of 10^8 across the different experiments—γ varies by less than a factor of 3. The inset in (a) illustrates that faster compression rates enable the metastable liquid to be undercooled further to states with a higher driving force $\Delta\mu/k_B T$ for solidification, analogous to how the restoring force in a spring becomes stronger as it gets increasingly stretched. This translates to reduced energy barriers $\Delta G^*/k_B T$, higher nucleation rates J of smaller but more densely packed clusters, faster growth rates γ, and shorter transition times τ, allowing for the possibility of solidification across multiple timescales.

$J = \mathcal{A}\exp(-\Delta G^*/k_B T)$, where the preexponential factor $\mathcal{A}$ largely reflects the availability of nucleation sites. Although $\mathcal{A}$ varies from one experiment to another, these differences are negligible compared to the overwhelming importance of $\exp(-\Delta G^*/k_B T)$, which dominates the high-pressure, homogeneous-nucleation regimes of interest in this study [5]. The variation exhibited by $\Delta G^*/k_B T$ in Fig. 3(a) is enough to explain the nearly 10^8 factor of difference in J across the different studies in Fig. 3(b). This 10^8 variation in J is consistent with the fact that the Kolmogorov time τ, which is a characteristic time associated with the phase transition [9,48], is proportional to

$J^{-1/4}$ so that τ varies by a factor of about $10^2 = (10^8)^{1/4}$ across the different experiments, as shown in Fig. 3(c). This 10^2 variation in τ matches the 10^2 variation in dP/dt. If τ were unaffected by dP/dt, solidification would not occur at higher compression rates, in contradiction to experimental observations. Thus, in summary, CNT posits that the larger undercooling (or equivalently, the smaller energy barrier $\Delta G^*/k_B T$) that one generally achieves with increasing dP/dt can translate to an orders-of-magnitude increase in the nucleation rate J, ultimately resulting in a characteristic transition time τ that scales proportionally with the time-scale of the experiment itself. This seemingly automatic

ability of the solidification process to "renormalize" itself is what enables solidification to be observed in all three experimental platforms examined in this study, despite the vastly different timescales associated with those platforms.

Finally, we briefly mention two applications of the scaling law, both of which are described further in the Supplemental Material [24]. On the first of these two applications, we note that although our study has focused on homogeneous nucleation, the analysis also has implications for designing experiments that primarily involve heterogeneous nucleation induced by dissolved impurities. By a simple extension of the arguments surrounding Fig. 3, the Supplemental Material [24] explains why heterogeneous nucleation becomes less prominent compared to homogeneous nucleation with increasing compression rates. Thus, even if heterogeneous nucleation is found to be negligible at high compression rates, say in a laser-drive experiment, one cannot necessarily conclude that it would also be unimportant at the lower compression rates of a gas-gun experiment. Conversely, if heterogeneous nucleation is found to be important in a gas-gun experiment, the same may not be true in a laser-drive experiment. The second application of the scaling law that we highlight here is, in our opinion, potentially more important. We have seen that the equilibrium melt properties P_{melt}, σ_{melt}, ρ_{melt}, and T_{melt} that underlie the dimensional analysis and scaling law in Eq. (1) can serve as good predictors of the observed nonequilibrium transition pressure P_{trans}. But what about the "reverse" direction? That is, if we have experimental information on P_{trans} as well as dP/dt, can we use that information together with the scaling law to infer P_{melt}, σ_{melt}, ρ_{melt}, and T_{melt} of a material where these melt properties are unknown? The Supplemental Material [24] shows that it is indeed possible to reliably infer the equilibrium melt temperature T_{melt} in this manner. It therefore provides an intriguing way to determine melt temperatures (i.e., temperatures along solid-liquid equilibrium phase boundaries) at high pressures, which is a topic of paramount importance that remains a long-standing challenge to this day.

Through the application of dimensional analysis to theoretical and experimental results (including our own Ga experiments) on nucleation and growth processes, we have derived a physics-based scaling law for how the timescale of solidification under homogeneous nucleation depends upon compression rate in both metallic and molecular systems. This renormalized theory for solidification under quasi-isentropic compression invites questions of whether a similar type of scaling approach could be useful for phase transitions via heterogeneous nucleation or along other compression paths, such as shock Hugoniots [49,50], which would complement the now well-known Swegle-Grady relation [51,52]. Prominent examples of such phase transitions are melt (solid-to-liquid) transitions [53], which are the opposite of the solidification processes considered in our study. Another interesting case for future consideration are solid–solid

transitions, where the mechanism may be governed not only by nucleation and growth but also dislocation-mediated processes (e.g., those that get manifested in material strength) [13,54,55]. The scaling law also raises the question of whether the most undercooled state theoretically possible, in which the nucleation barrier $\Delta G^*/k_B T = 1$, could be accessed at extreme compression rates that lie far beyond any experimental method currently available. We encourage future atomistic simulations and experiments to explore these questions and to further test, refine, and apply the scaling law on a wider range of materials and nonequilibrium settings.

---

[*]These authors contributed equally to this work.
[†]belof1@llnl.gov

[1] A. Lazicki *et al.*, Metastability of diamond ramp-compressed to 2 terapascals, Nature (London) **589**, 532 (2021).

[2] R. F. Smith *et al.*, Ramp compression of diamond to five terapascals, Nature (London) **511**, 330 (2014).

[3] R. G. Kraus *et al.*, Measuring the melting curve of iron at super-Earth core conditions, Science **375**, 202 (2022).

[4] M. C. Marshall *et al.*, Metastability of Liquid Water Freezing into Ice VII Under Dynamic Compression, Phys. Rev. Lett. **127**, 135701 (2021).

[5] P. C. Myint, A. A. Chernov, B. Sadigh, L. X. Benedict, B. M. Hall, S. Hamel, and J. L. Belof, Nanosecond Freezing of Water at High Pressures: Nucleation and Growth Near the Metastability Limit, Phys. Rev. Lett. **121**, 155701 (2018).

[6] D. H. Dolan, M. D. Knudson, C. A. Hall, and C. Deeney, A metastable limit for compressed liquid water, Nat. Phys. **3**, 339 (2007).

[7] D. Kashchiev, *Nucleation: Basic Theory with Applications*, 1st ed. (Butterworth-Heinemann, Oxford, 2000),

[8] S. Toschev, Homogeneous nucleation, *Chapter 1 of Crystal Growth: An Introduction* (North-Holland Publishing, Amsterdam, 1973), pp. 1–49.

[9] A. A. Chernov *et al.*, *Modern Crystallography III: Crystal Growth*, Vol. 36 of Springer Series in Solid-State Sciences (Springer-Verlag, Berlin and Heidelberg, 1984).

[10] E. Clouet, *Modeling of Nucleation Processes* (ASM Handbook, 2009), Vol. 22A, p. 203, 10.31399/asm.hb.v22a.a0005410.

[11] K. F. Kelton and A. L. Greer, *Nucleation in Condensed Matter: Applications in Materials and Biology* (Pergamon Publications, Oxford, 2010).

[12] J. Edwards *et al.*, Laser-Driven Plasma Loader for Shockless Compression and Acceleration of Samples in the Solid State, Phys. Rev. Lett. **92,** 075002 (2004).

[13] E. E. McBride *et al.*, Phase transition lowering in dynamically compressed silicon, Nat. Phys. **15,** 89 (2019).

[14] C. A. Hall, J. R. Asay, M. D. Knudson, W. A. Stygar, R. B. Spielman, T. D. Pointon, D. B. Reisman, A. Toor, and R. C. Cauble, Experimental configuration for isentropic compression of solids using pulsed magnetic loading, Rev. Sci. Instrum. **72,** 3587 (2001).

[15] T. S. Duffy and R. F. Smith, Ultra-high pressure dynamic compression of geological materials, Front. Earth. Sci. **7,** 23 (2019).

[16] D. H. Dolan and Y. M. Gupta, Nanosecond freezing of water under multiple shock wave compression: Optical transmission and imaging measurements, J. Chem. Phys. **121,** 9050 (2004).

[17] G. E. Duvall and R. A. Graham, Phase transitions under shock-wave loading, Rev. Mod. Phys. **49,** 523 (1977).

[18] S. J. P. Stafford, An experimental study on the dynamic compression and subsequent freezing of water, Ph.D. thesis, Imperial College London, Department of Physics, 2016, p. 223, https://spiral.imperial.ac.uk/handle/10044/1/44071.

[19] S. J. P. Stafford, D. J. Chapman, S. N. Bland, and D. E. Eakins, Observations on the nucleation of ice VII in shock compressed water, AIP Conf. Proc. **1793,** 130005 (2017).

[20] E. J. Nissen and D. H. Dolan, Temperature and rate effects in ramp-wave compression freezing of liquid water, J. Appl. Phys. **126,** 015903 (2019).

[21] D. H. Dolan, J. N. Johnson, and Y. M. Gupta, Nanosecond freezing of water under multiple shock wave compression: Continuum modeling and wave profile measurements, J. Chem. Phys. **123,** 064702 (2005).

[22] M. Bastea, S. Bastea, J. E. Reaugh, and D. B. Reisman, Freezing kinetics in overcompressed water, Phys. Rev. B **75,** 172104 (2007).

[23] A. E. Gleason *et al.*, Compression Freezing Kinetics of Water to Ice VII, Phys. Rev. Lett. **119,** 025701 (2017).

[24] See Supplemental Material at http://link.aps.org/supplemental/10.1103/PhysRevLett.131.106101 for more details on the dimensional analysis procedure, applications of the scaling law, and our magnetic-drive experiments on gallium. The Supplemental Material includes Refs. [25–38].

[25] L. M. Barker and R. E. Hollenbach, Laser interferometer for measuring high velocities of any reflecting surface, J. Appl. Phys. **43,** 4669 (1972).

[26] R. M. Darlington, T. L. McAbee, and G. Rodrigue, A study of ALE simulations of Rayleigh–Taylor instability, Comput. Phys. Commun. **135,** 58 (2001).

[27] V. A. Dobrev, T. V. Kolev, and R. N. Rieben, High-order curvilinear finite element methods for Lagrangian hydrodynamics, SIAM J. Sci. Comput. **34,** B606 (2012).

[28] F. Pedregosa *et al.*, SCIKIT-LEARN: Machine learning in PYTHON, J. Mach. Learn. Res. **12,** 2825 (2011), https://scikit-learn.org/stable/about.html.

[29] J. Kennedy and R. Eberhart, Particle swarm optimization, in *Proceedings of the IEEE International Conference on Neural Networks* (Perth, Australia, 1995), pp. 1942–1948.

[30] P. C. Myint, L. X. Benedict, C. J. Wu, and J. L. Belof, Minimization of Gibbs energy in high-pressure multiphase, multicomponent mixtures through particle swarm optimization, ACS Omega **6,** 13341 (2021).

[31] Y. Ping *et al.*, Solid Iron Compressed up to 560 GPa, Phys. Rev. Lett. **111,** 065501 (2013).

[32] S. J. Turneaure, S. M. Sharma, and Y. M. Gupta, Crystal Structure and Melting of Fe Shock Compressed to 273 GPa: *In situ* X-Ray Diffraction, Phys. Rev. Lett. **125,** 215702 (2020).

[33] D. A. Brantley, R. S. Crum, and M. C. Akin, Comparing temperature convergence of shocked thin films of tin and iron to a bulk temperature source, J. Appl. Phys. **129,** 015903 (2021).

[34] D. Reisman *et al.*, Pulsed power accelerator for material physics experiments, Phys. Rev. ST Accel. Beams **18,** 090401 (2015).

[35] R. Stumpf and P. J. Feibelman, Towards an understanding of liquid-metal embrittlement: Energetics of Ga on Al surfaces, Phys. Rev. B **54,** 5145 (1996).

[36] S. D. Crockett and S. Rudin, Lithium fluoride equations of state (SESAME 7271), Technical Report No. LA-UR-06-8401, Los Alamos National Laboratory, 2006, http://permalink.lanl.gov/object/view?what=info:lanl-repo/lareport/LA-UR-06-8401.

[37] R. W. Lemke, M. D. Knudson, A. C. Robinson, T. A. Haill, K. W. Struve, J. R. Asay, and T. A. Mehlhorn, Self-consistent, two-dimensional, magnetohydrodynamic simulations of magnetically driven flyer plates, Phys. Plasmas **10,** 1867 (2003).

[38] J. L. Brown, C. S. Alexander, J. R. Asay, T. J. Vogler, D. H. Dolan, and J. L. Belof, Flow strength of tantalum under ramp compression to 250 GPa, J. Appl. Phys. **115,** 043530 (2014).

[39] G. I. Barenblatt, *Scaling* (Cambridge University Press, Cambridge, England, 2003).

[40] Y. A. Cengel and J. M. Cimbala, *Fluid Mechanics: Fundamentals and Applications* (McGraw-Hill, New York, 2018).

[41] P. C. Myint, L. X. Benedict, and J. L. Belof, Free energy models for ice VII and liquid water derived from pressure, entropy, and heat capacity relations, J. Chem. Phys. **147,** 084505 (2017).

[42] P. C. Myint and J. L. Belof, Rapid freezing of water under dynamic compression, J. Phys. Condens. Matter **30,** 233002 (2018).

[43] D. M. Sterbentz, P. C. Myint, J.-P. Delplanque, and J. L. Belof, Numerical modeling of solid-cluster evolution applied to the nanosecond solidification of water near the metastable limit, J. Chem. Phys. **151,** 164501 (2019).

[44] D. M. Sterbentz, J. R. Gambino, P. C. Myint, J.-P. Delplanque, H. K. Springer, M. C. Marshall, and J. L. Belof, Drive-pressure optimization in ramp-wave compression experiments through differential evolution, J. Appl. Phys. **128,** 195903 (2020).

[45] P. C. Myint, B. Sadigh, L. X. Benedict, D. M. Sterbentz, B. M. Hall, and Jonathan L. Belof, Coupling solidification kinetics with phase-behavior computations in hydrodynamic simulations of high-pressure, dynamic-compression processes, AIP Adv. **10,** 125111 (2020).

[46] C. J. Prisbrey and C. J. Wu, Multiphase EOS table for gallium, in *Proceedings of the APS March Meeting* (American Physical Society, Denver, CO, USA, 2020), https://meetings.aps.org/Meeting/MAR20/Session/M03.1. This EOS is currently being refined and finalized for journal submission. An electronic version of the EOS in tabular format may be available upon reasonable request.

[47] D. M. Sterbentz, P. C. Myint, J.-P. Delplanque, Y. Hao, J. L. Brown, B. S. Stoltzfus, and J. L. Belof, A model for the solid–liquid interfacial free energy at high pressures, Langmuir **38,** 9892 (2022).

[48] A. N. Kolmogorov, *On The Statistical Theory of Metal Crystallization*, Vol. 26 of Mathematics and Its Applications (Soviet Series), Chapter 22 of Selected Works of A. N. Kolmogorov. Volume II: Probability Theory and Mathematical Statistics, edited by A. N. Shiryayev (Springer, Dordrecht, 1992), pp. 188–192, translated by G. Lindquist.

[49] A. E. Gleason *et al.*, Ultrafast visualization of crystallization and grain growth in shock-compressed SiO_2, Nat. Commun. **6,** 8191 (2015).

[50] T. Wei, S. Lim, and Y. Wang, Scaling of Hugoniot curves for shock-compressed liquids, J. Appl. Phys. **128,** 235901 (2020).

[51] J. W. Swegle and D. E. Grady, Shock viscosity and the prediction of shock wave rise times, J. Appl. Phys. **58,** 692 (1985).

[52] Y. Horie, Observations on the fourth-power scaling of high-pressure shock waves in solids, J. Appl. Phys. **130,** 245901 (2021).

[53] P. Renganathan, S. M. Sharma, S. J. Turneaure, and Y. M. Gupta, Real-time (nanoseconds) determination of liquid phase growth during shock-induced melting, Sci. Adv. **9,** eade5745 (2023).

[54] M. G. Gorman *et al.*, Direct Observation of Melting in Shock-Compressed Bismuth with Femtosecond X-Ray Diffraction, Phys. Rev. Lett. **115,** 095701 (2015).

[55] J. S. Wark, M. I. McMahon, and J. H. Eggert, Femtosecond diffraction and dynamic high pressure science, J. Appl. Phys. **132,** 080902 (2022).